

The FFX Correlator

Satoru IGUCHI ¹ and Takeshi OKUDA ¹

¹*National Astronomical Observatory, 2-21-1 Osawa, Mitaka, Tokyo 181-8588*
s.iguchi@nao.ac.jp
takeshi.okuda@nao.ac.jp

(Received 2007 November 1; accepted 2008 April 13)

Abstract

We established a new algorithm for correlation process in radio astronomy. This scheme consists of the 1st-stage Fourier Transform as a filter and the 2nd-stage Fourier Transform for spectroscopy. The "FFX" correlator stands for Filter and FX architecture, since the 1st-stage Fourier Transform is performed as a digital filter, and the 2nd-stage Fourier Transform is performed as a conventional FX scheme. We developed the FFX correlator hardware not only for the verification of the FFX scheme algorithm but also for the application to the Atacama Submillimeter Telescope Experiment (ASTE) telescope toward high-dispersion and wideband radio observation at submillimeter wavelengths. In this paper, we present the principle of the FFX correlator and its properties, as well as the evaluation results with the production version.

Key words: techniques: spectroscopic— instrumentation: spectrographs— radio continuum: general— radio lines: general— instrumentation: interferometers

1. Introduction

The signals received by the antennas obey the stationary stochastic process and then ergodic process. The ergodic theory can be applied to the auto-correlation function for a spectrometer and the cross-correlation function for radio interferometer. Under such conditions, Weinreb (1963) developed the first digital spectrometer. This digital spectrometer is called the XF correlator in which the correlation is calculated before Fourier Transform. Meanwhile, Chikada et al. (1987) developed the first the FX correlator of an another design, in which Fourier Transform is performed before cross multiplication. Although there is a difference of property between two basic designs, the obtained astronomical spectra of them were confirmed to be identical.

Determining the number of correlation lags in the XF scheme or of Fourier Transform points in the FX scheme is essential for the realization of high-dispersion and wideband observation, because the frequency resolution is derived as

$$\Delta f = 1/(\Delta t_s N) = 2B/N, \quad (1)$$

where Δt_s is the sampling period, N is the number of correlation lags or Fourier Transform points, and the bandwidth of B is equal to $1/(2\Delta t_s)$. The material size and cost of the correlator strongly depend on the sampling period, Δt_s , and the number of correlation lags or Fourier Transform points, N .

The new XF architecture with the digital Tunable Filter Bank that is designed with the Finite Impulse Response (FIR) has been proposed and developed for the next generation radio interferometers, the Expanded Very Large Array (EVLA) and the Atacama Large Millimeter/submillimeter Array (ALMA) (Carlson 2001,

Escoffier et al. 2007). This is called the "FXF correlator". The architecture of the FXF scheme can make the material size smaller in comparison with that of the conventional XF scheme. Since the digital filter allows a variety of observation modes [scientific and observational availability were shown in Iguchi et al. (2004)], the FXF scheme will provide us with the most appropriate specifications which meet the scientific requirements. This will lower the risk of over-engineering of the correlator.

The improved FX architecture with DFT filterbank was developed by Bunton (2000). The use of polyphase filter banks allows arbitrary filter responses to be implemented in the FX scheme (Bunton 2003). This is called the "Polyphase FX Correlator". This scheme has a possibility to achieve the spectral leakage of about -120 dB. In particular, this performance is significant to suppress the leakage from the spurious lines mixed in receiving, down-converting or digitizing.

The FFX Correlator is a new algorithm for correlation process in radio astronomy. The FFX scheme consists of 2-stage Fourier Transform blocks, which perform the 1st-stage Fourier Transform as a digital filter, and the 2nd-stage Fourier Transform to achieve higher dispersion. The first 'F' of the FFX is the initial letter of the word "Filter". In this paper, we present a new FFX architecture. The principle of the FFX scheme in section 2, the properties of the FFX scheme in section 3, the algorithm verification and performance evaluation with the developed FFX correlator in sections 4 and 5, and the summary of this paper in section 6 are presented.

2. Principle of the FFX Correlator

This section shows the algorithm and the data flow diagram of the signal processing in the Fourier Transform of

the FFX scheme (see figure 1). Suppose that x_n are the digital waveforms at the correlator input from the astronomical radio signals that are received by the telescope. The inputs, x_n , are real digital signals at sampling period of Δt_s , and obey the zero-mean Gaussian random variable. The suffix n is an integer for time.

[Step 1] The correlator receives the time-domain digital sampling signals from the Analog-to-Digital Converter (ADC), and accumulate them up to N_n points.

[Step 2] The time-domain N_n -point data are transferred to the frequency-domain by using the N_n -point Discrete Complex Fourier Transform as follows:

$$X_p = \Delta t_s \sum_{n=0}^{N_n-1} x_n \exp\left(-j \frac{2\pi p n}{N_n}\right), \quad (2)$$

where X is the spectrum after the 1st Fourier Transform, the suffix p is an integer for frequency, and Δt_s is equal to $1/(2B_{1st})$ at the bandwidth of B_{1st} . The Δf_{1st} is the minimum frequency resolution of the 1st Fourier Transform, which is equal to $1/(\Delta t_s N_n)$.

[Step 3] The extraction of the N_k points from the frequency domain $N_n/2$ -point data after the 1st Fourier Transform is conducted as if filter and frequency conversion are performed simultaneously:

$$X'_k = X_p \quad (p = k + k_0, \quad k = 0, \dots, N_k - 1), \quad (3)$$

where k_0 is the minimum frequency channel in the extraction, and the suffix k is an integer for frequency.

[Step 4] The N_k -point data after Inverse Fourier Transform is written by

$$x'_l = \frac{1}{\Delta t_f N_k} \sum_{k=0}^{N_k-1} X'_k \exp\left[j \frac{2\pi(k - N_k/2)l}{N_k}\right], \quad (4)$$

where x' is the time-domain signal after inverse Fourier Transform, the suffix l is an integer for time, and Δt_f is the sampling period after filtering at the bandwidth of B_{2nd} ($\Delta t_f = 1/B_{2nd} = 1/\Delta f_{1st} N_k$).

[Step 5] By repeating the procedure from Step 1 to Step 4, the data are gathered up to N_m points as follows;

$$x'_m = x'_{l+dN_k} \quad (5)$$

where m is $l + dN_k$, and d is the number of repeating times of the procedure from Step 1 to Step 4.

[Step 6] The time-domain N_m -point data after gathering are transferred to the frequency-domain by using the N_m -point Discrete Complex Fourier Transform as follows:

$$X'_q = \Delta t_f \sum_{m=0}^{N_m-1} x'_m \exp\left(-j \frac{2\pi q m}{N_m}\right), \quad (6)$$

where X' is the spectrum after the 2nd Fourier Transform, and the suffix q is an integer for frequency. The Δf_{2nd} is the minimum frequency resolution after the 2nd Fourier Transform, which is equal to $1/(\Delta t_f N_m)$ ($=\Delta f_{1st} N_k/N_m$).

The definition of all functions used in this section is summarized in table 1. Also, the summary of the relationship among the functions (see table 1) is listed in table 2. The following relations are derived:

Table 1. Definition of functions.

Mark	Explanation
B_{1st}	Bandwidth of the input signals
Δt_s	Sampling period of the input signals
N_n	Number of the points of 1st FT
Δf_{1st}	Minimum frequency resolution of 1st FT
N_k	Number of the extraction times as a filter
B_{2nd}	Bandwidth after extraction
Δt_f	Sampling period after filtering
N_m	Number of the points of 2nd FT
Δf_{2nd}	Minimum frequency resolution of 2nd FT

Note that FT is Fourier Transform.

Table 2. Relationship among the functions (see table 1).

Equation	
(a)	$\Delta t_s = 1/(2B_{1st})$
(b)	$\Delta f_{1st} = 2B_{1st}/N_n$ $= 1/(\Delta t_s N_n)$
(c)	$\Delta t_f = 1/B_{2nd}$ $= 1/(\Delta f_{1st} N_k)$ $= \Delta t_s N_n/N_k$
(d)	$\Delta f_{2nd} = B_{2nd}/N_m$ $= 1/(\Delta t_f N_m)$ $= \Delta f_{1st} N_k/N_m$ $= 2B_{1st}/N_n \cdot N_k/N_m$

$$\Delta f_{1st} = 2B_{1st}/N_n, \quad (7)$$

$$\Delta f_{2nd} = 2B_{1st}/N_n \cdot N_k/N_m. \quad (8)$$

The frequency resolution of the FFX scheme is determined by the number of of the 1st Fourier Transform points(N_n), the number of the extractions as a filter (N_k), and the number of the 2nd Fourier Transform points(N_m).

3. Properties of the FFX Correlator

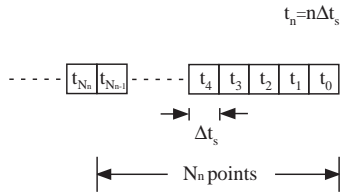
The frequency responses for spectroscopic observations are finally derived by Fourier Transform in all schemes. For finite length of Fourier Transform, the responses are multiplied by a rectangular window function, which corresponds to convolving sinc function in the frequency domain. The frequency profile of the XF scheme becomes the shape of sinc function profile, while that of the FX scheme is sinc squared function profile. This indicates the FX scheme (including the FFX and polyphase FX schemes) is better than the XF scheme (including the FXF scheme) from the view points of the frequency profile and sharpness of individual frequency channels, and the spectral leakage.

For the realization of the high frequency resolution in the conventional FX scheme, the N -point complex FFT may be divided into $N/2$ -point FFTs, N -point twiddle factor multiplications, and $N/2$ -point second FFTs, because the circuit size of the LSI (Large-Scale Integration) is limited (Iguchi et al. 2002). The memory and circuit for the twiddle factor multiplications are critical. However,

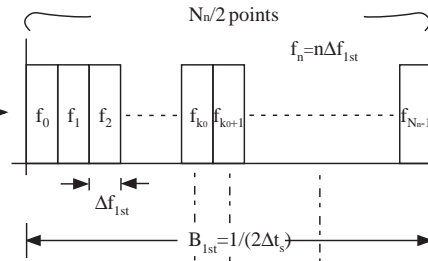
Fig1

N_n -point Discrete Complex Fourier Transform

[Step 1] Time domain N_n -point data



[Step 2] Frequency domain $N_n/2$ -point data after Fourier Transform

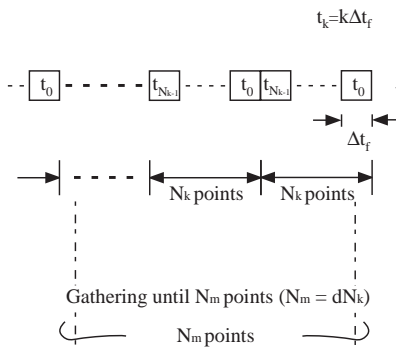


Extracting N_k -point frequency components.

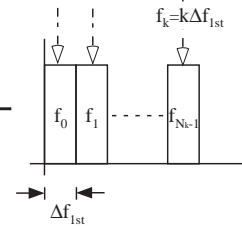


N_k -point Inverse Discrete Complex Fourier Transform

[Step 4] Time domain N_k -point data after Inverse Fourier Transform

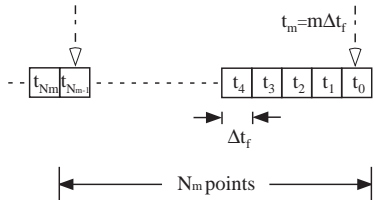


[Step 3] Extraction of the N_k -point frequency components



N_m -point Discrete Complex Fourier Transform

[Step 5] Time domain N_m -point data after gathering



[Step 6] Frequency domain N_m -point data after 2nd Fourier Transform

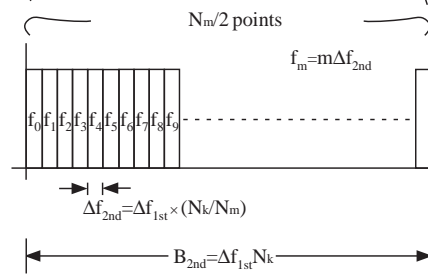


Fig. 1. Algorithm and the data flow diagram of the FFX scheme.

the high frequency resolution can be realized in the FFX scheme without the twiddle factor multiplications.

The FFX scheme has advantages of selectivity for frequency resolution and bandwidth in comparison with other schemes. The comparable functions are also realized by implementing a digital LO circuits (Escoffier et al. 2007). The digital LO circuits need to be delicately designed to avoid the spurious in mixing the digital LO signals due to the rounding errors in the calculation process.

For the investigation of aliasing or foldover from frequencies over the bandedge in the FFX scheme, it is necessary and important to estimate the frequency response. As shown in [Step 3] in figure 1, the desired frequency response, equation (3) can be rewritten as

$$X'_k = X'_p \quad (p = k + k_0, \quad k = 0, \dots, N_k - 1), \quad (9)$$

$$X'_p = H_p \cdot X_p, \quad (10)$$

$$H_p = \begin{cases} 1 & (p = k_0, \dots, k_0 + N_k - 1) \\ 0 & (p < k_0, \quad p > k_0 + N_k - 1). \end{cases} \quad (11)$$

However, " H_{k_0} " should be replaced by zero to reduce the aliasing or foldover of noise from frequencies over the bandedge. Thus, in the FFX scheme, equation (11) need to be replaced as

$$H_p = \begin{cases} 1 & (p = k_0 + 1, \dots, k_0 + N_k - 1) \\ 0 & (p < k_0 + 1, \quad p > k_0 + N_k - 1). \end{cases} \quad (12)$$

According to the two (1st and inverse) Fourier Transforms at the same resolution, the actual designed transfer function of the impulse response, which is derived with the square of sinc function, is represented as follows:

$$|H(f)| = \sum_{p=0}^{N_n-1} H_p^2 \left\{ \frac{\sin[\pi(N_n \Delta t_s f - p)]}{\pi(N_n \Delta t_s f - p)} \right\}^2, \quad (13)$$

$$P(f) = \left\{ \sum_{p=0}^{N_n-1} H_p^2 \left\{ \frac{\sin[\pi(N_n \Delta t_s f - p)]}{\pi(N_n \Delta t_s f - p)} \right\}^2 \right\}^2, \quad (14)$$

where f is an arbitrary frequency, and also the response of a sinc function is caused by one Fourier Transform. It can be confirmed that the designed transfer function approaches the desired frequency response by increasing N_n while keeping N_n/N_k constant. The filtering process in the FFX scheme is similar to that used in the design method of a Frequency Sampling Filter, FSF (Rabiner and Schafer 1971).

Also, to improve the frequency response, the window function before 1st Fourier Transform can be multiplied. In that case, equation (14) should be written as

$$|H(f)| = \sum_{p=0}^{N_n-1} H_p^2 W(N_n \Delta t_s f - p) \frac{\sin[\pi(N_n \Delta t_s f - p)]}{\pi(N_n \Delta t_s f - p)}, \quad (15)$$

$$P(f) = \left\{ \sum_{p=0}^{N_n-1} H_p^2 W(N_n \Delta t_s f - p) \frac{\sin[\pi(N_n \Delta t_s f - p)]}{\pi(N_n \Delta t_s f - p)} \right\}^2, \quad (16)$$

where $W(f)$ is the response after the window function $w(n)$ is transferred to the frequency-domain by Fourier Transform. If the window is a rectangular window function, $W(f)$ becomes a sinc function. In that case, equation (16) consists with equation (14). There are the following famous window functions: Hanning, Hamming, Blackman, and Kaiser. By well making a choice of the window function, the first sidelobe of stopband in the frequency response will be improved. It is well known that the first sidelobe levels with Backman and Kaiser as the window are better than those Hanning and Hamming. For the FFX scheme, it is found that the Bessel function of zeroth order J_0 is better than others. This frequency response is shown in figure 2. The first and second sidelobe levels is about -34 dB, the fifth and sixth sidelobe levels is about -50 dB, and higher-order sidelobe levels will be better than -60 dB (see figure 2a). The stopband response of the FFX scheme is not better than that of the polyphase FX scheme (Bunton 2000) and that of the FXF scheme for EVLA (Carlson 2001). On the other hand, the ripple response in the passband is less than 0.4 dB peak-to-peak (see figure 2b). This performance is better than that of the polyphase FX scheme.

Note that the stopband performance to suppress the spurious lines can be improved by installing "the detection and cancellation techniques of high and low frequency spurious lines" into the FFX scheme (Chikada found this algorithm in the development of ALMA/ACA correlator).

4. Requirements and Specifications for the Development of the FFX Correlator

The development of the FFX correlator hardware is significant for the verification of the FFX scheme algorithm. It is necessary to define the requirements and specifications of the hardware of the FFX correlator. The hardware size can be optimized for the verification of algorithm. On the other hand, there were the scientific requests for the application to the Atacama Submillimeter Telescope Experiment (ASTE), which is a new project to install and operate a 10-m submillimeter telescope at a high latitude site (4,800 m) in the Atacama desert in northern Chile (Ezawa et al. 2004). Under these situations, the FFX correlator hardware for the algorithm verification was specified by also considering the scientific requirements for submillimeter astronomy including the application to ASTE.

In case of spectroscopic observations of atomic / molecular line emissions, their line width are extended by the Doppler shift along a line of sight with movement of inter stellar matter (ISM). In nuclear regions of external galaxies and Ultra Luminous Infrared Galaxies (ULIRGs), the molecular clouds which have various velocity components can be observed simultaneously, and line widths of the observed atomic / molecular emission lines are extended. For example, the line width of CO line emission of external galaxy is sometimes extended to more than 800 km s⁻¹ (i.e. Narayanan et al. 2005), which corresponds to about 920 MHz in ¹²CO(J=3-2) ($\nu_{\text{rest}} \sim 345.796$ GHz) and about

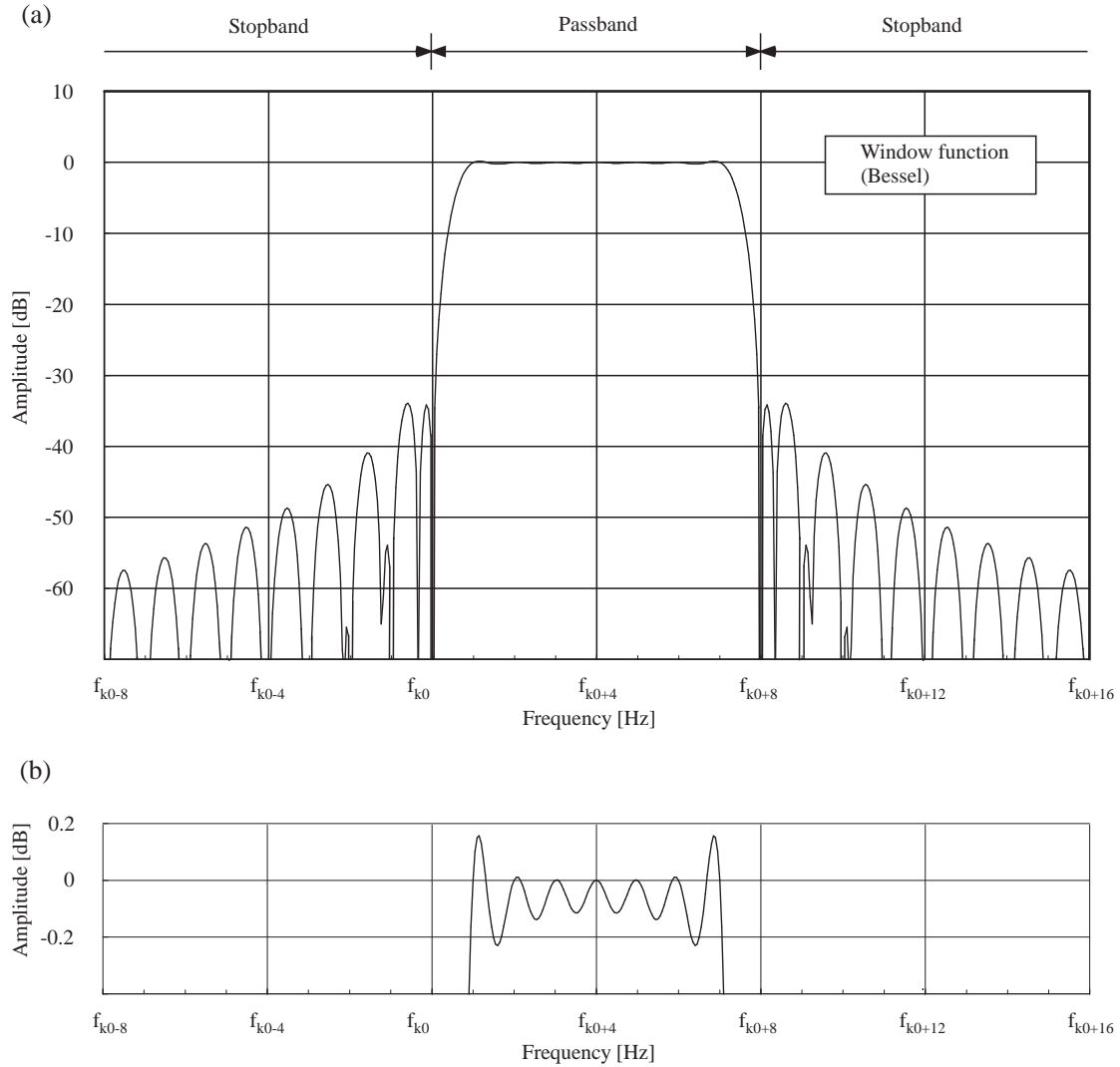


Fig. 2. The frequency response of 1st FFT stage in the FFX scheme, which works as a digital filter. (a) is the frequency response at the full range to investigate the stopband, and (b) is the closeup frequency response in the passband to investigate a ripple. The frequency response is multiplied by the window of the Bessel function, $w(n) = J_0\left(\frac{4.24n}{N_n}\right)$.

Table 3. FFT segment length.

FFT stage	FFT segment length
First stage FFT	1024 points
Inverse FFT	8 points
Second stage FFT	4096 points

2.2 GHz in $^{12}\text{CO}(J=7-6)$ ($\nu_{\text{rest}} \sim 806.652$ GHz), by rotating around its nuclear region. On the other hand, in order to evaluate the kinematics of protoplanetary disks and the internal structure of molecular clouds in the Milky Way, it is also necessary to resolve their thermal line widths using spectrometer with high frequency dispersion; for instance, frequency resolution of 32 kHz corresponds to velocity resolution of 0.032 km s^{-1} at 1 mm wave length.

As the full bandwidth of more than 3 GHz is required, the FFX correlator need to achieve the processing speed

of 8192 Mega sample per second (Msps). In that case, for the realization of two-type spectral resolutions of about 5 MHz and less than 32 kHz, the FFX correlator must meet at least the specifications in table 3.

5. Development and Evaluation of the FFX Correlator

The correlation processing block diagram of the FFX correlator is shown in figure 3. The FFX correlator consists of DTS-R (Data Transmission System Receiver) module, Correlation Module, and the Monitor & Control Computer. In the DTS-R module, the DTS-R Board or the ADC (Analog-to-Digital Converter) Board is implemented as an EIB (Electrical input Interface Board). The input data rate of the FFX correlator is about 48 Giga bit per second (Gbps) with 3-bit quantization at the sampling frequency of 8192 or 4096 Msps, which is $8192 \text{ Msps} \times 3$

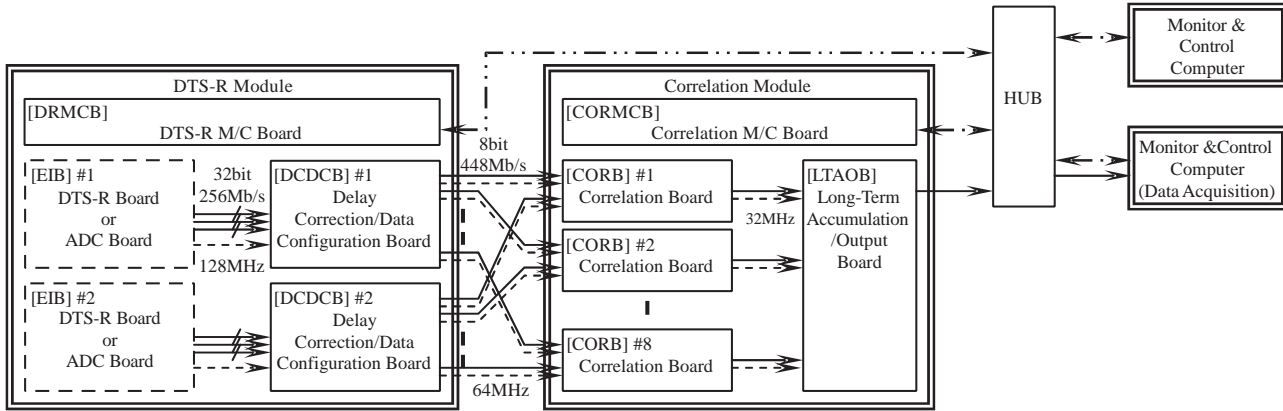


Fig. 3. Correlation processing block diagram of the FFX scheme.

bits \times 2 IF or 4096 Msps \times 3 bits \times 4 IFs. The DCDCB (Delay Correction and Data Configuration Board) effectively distributes the input signals to the next boards for the parallel correlation processing. For the data processing at the throughput of 8192 Msps, the correlation is performed with 16 parallels, and both of the real and imaginary parts are used in FFT. The data is sent to each 16-parallel CORB (Correlation Board) per one-segment length. In the correlation mode of the FFX scheme, the data is sent per total segment length which is determined considering the signal process including the second stage of FFT. Final correlation output is obtained by adding 16-parallel correlation results. The correlation output is sent to the Monitor & Control Computer via LAN cable. Switching between the FX processing and the FFX processing is normally operated by setting the command into the Monitor & Control Computer.

The correlation processing flow of the FFX correlator is shown in figure 4. All main logics are implemented in FPGAs (Field Programmable Gate Array).

5.1. Delay Correction and Data Configuration Board (DCDCB)

5.1.1. Delay Correction

The FFX correlator has a delay correction circuit per bit for every 3-bit sampling signal. Delay tracking for every single bit is realized by extracting 64-sample length from time-sequential 128 samples that are produced by splitting the output from FIFO (First In, First Out) memory in two, and shifting one side or the other in one-clock phase (see figure 5). Delay correction circuit has a FIFO memory of 1.024 Mega samples to each bit for delay tracking. In case of 8192 Msps, the delay correction range is ± 512 kilo samples, that is $\pm 62.5 \mu\text{sec}$ ($=\pm 18.75 \text{ km}$).

5.1.2. Data Distribution

Given the operation speed of the device (FPGA etc.), 16-parallel correlation processing is essential to achieve the throughput of 8192 Msps. To do this, the input signals are divided by one segment length of FFT and sent to the Correlation Board (CORB) so that each parallel processing is performed separately.

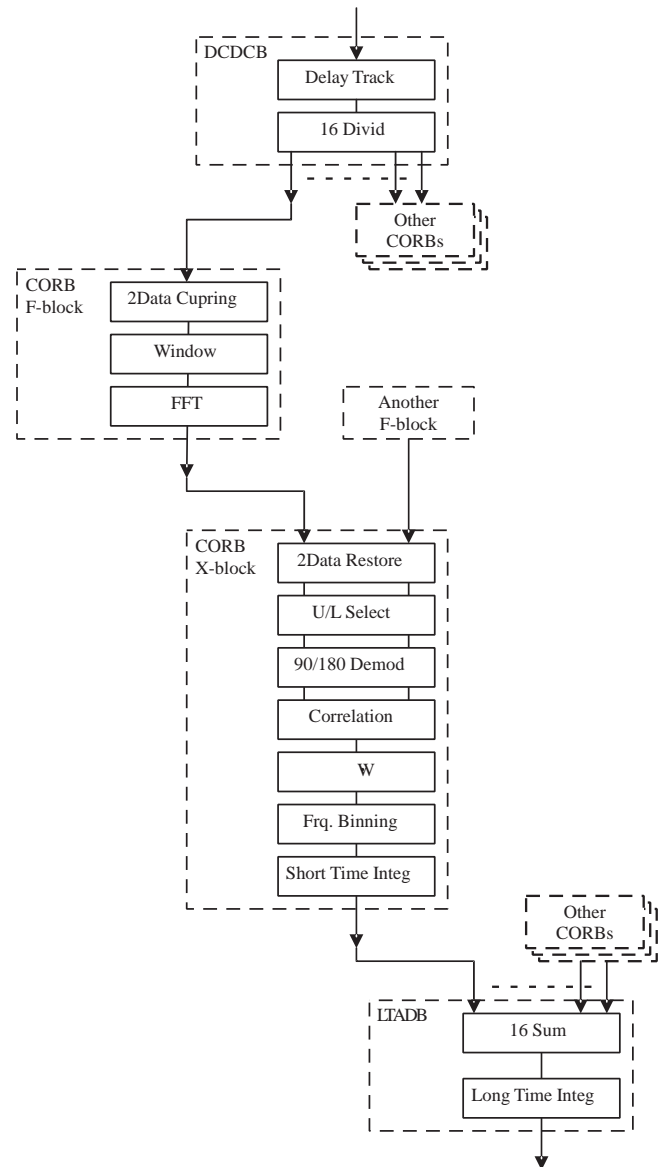


Fig. 4. Logical correlation processing flow.

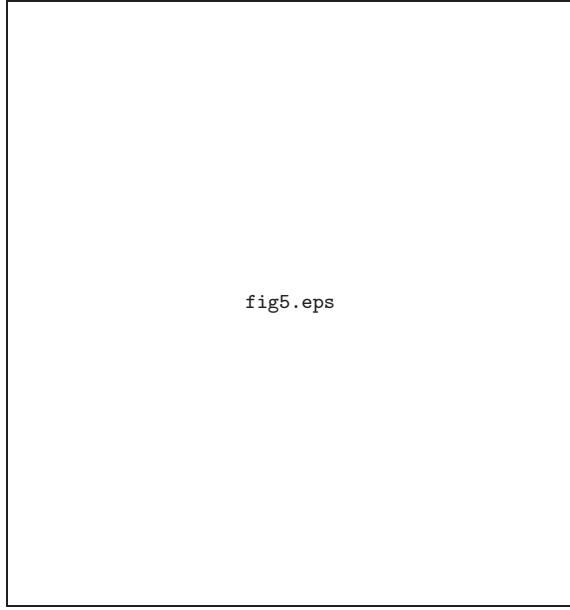


Fig. 5. Delay Correction.

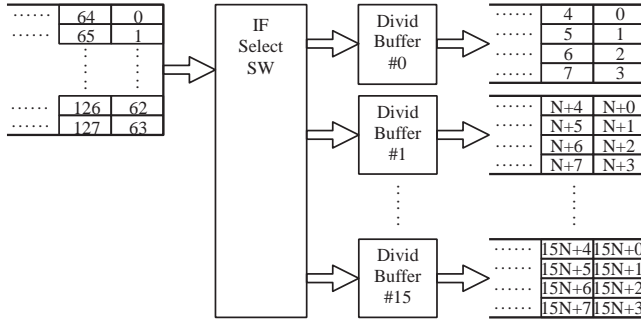


Fig. 6. Data Configuration.

In the FFX processing, the data is divided by single segment length of the second-stage FFT. From table 3, the input signals are divided into:

$$1024 \times 4096/8 = 512 \hat{k}, \quad (17)$$

where \hat{k} is 1024 (2^{10}). This value determines the one segment length of this FFT processing. 64-parallel signals are converted to 4-parallel after being output to each distribution buffer (see figure 6).

5.2. Correlation Board (CORB)

5.2.1. Operation Format

The operations of the correlation processing are performed using 16-bit floating point format. FFT calculation is expressed as

$$-1^s \cdot 2^{e-16} \cdot (1 + ma/1024), \quad (18)$$

and the range is from $\pm 1/32768$ to 131008. When the index (e) is 0, it is regarded as 0 instead of 2^{-16} irrespective of mantissa.

This not only simplifies the processing but also improves

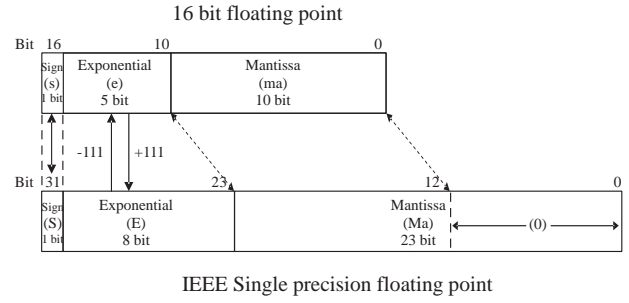


Fig. 7. Conversion between 16-bit floating point and IEEE single precision floating point.

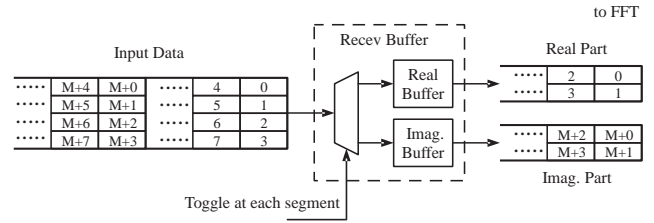


Fig. 8. Parallel processing of two datasets in FFT.

the compatibility with IEEE single precision floating point data. IEEE single precision floating point has 32-bit representing sign (S): 1 bit, exponential (E): 8 bits, and mantissa (Ma): 23 bits, and is expressed as

$$-1^S \cdot 2^{E-127} \cdot (1 + M/223), \quad (19)$$

and they have following relations

$$S = s, \quad (20)$$

$$E = e + 111, \quad (21)$$

$$Ma = ma \times 8192(2^{13}). \quad (22)$$

Conversion between 16-bit floating point and IEEE single precision floating point is also shown in figure 7.

5.2.2. Parallel processing of two datasets

Since FFT is the linear response, the real and imaginary parts of the input can be used separately. Since the signals received by an antenna are real part only, two datasets are combined into one complex dataset for the FFT processing (see figure 8). One dataset is inserted into a real part, and then next dataset is inserted into an imaginary part. These two datasets are shifted with one-FFT segment length (M), and then processed as one complex data. Combination of two datasets is performed by Read/Write sequence control of the received buffer (=input buffer in FPGA). This method can reduce the material size of the correlator.

5.2.3. F-Block (FX mode)

The FX processing is performed with $16\hat{k}$ -point FFT. In terms of the throughrate, pipeline processing is applied to each FFT stage processing. To reduce the memory size in the pipeline processing, $16\hat{k}$ -point FFT is realized by

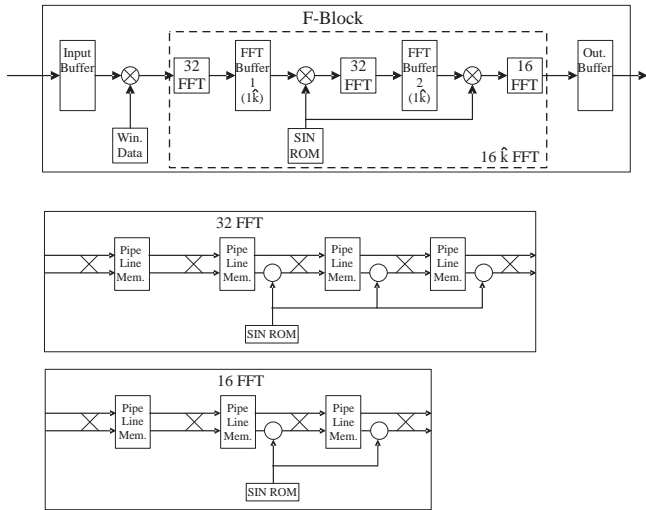


Fig. 9. Pipeline processing of the FX scheme ($16\hat{k}$ -point FFT).

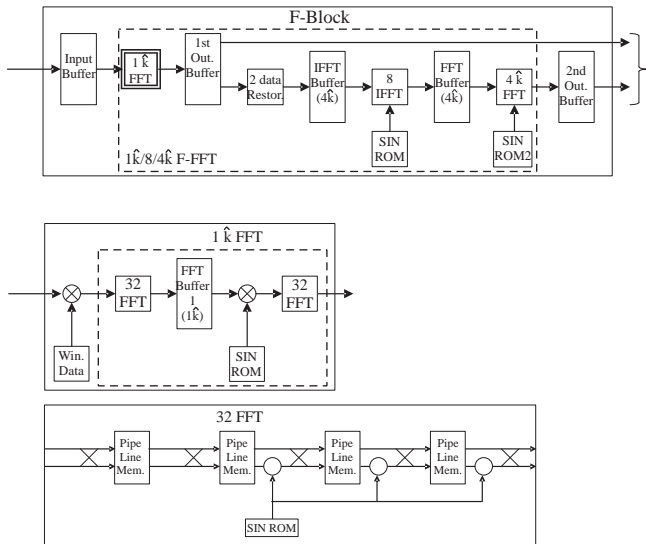


Fig. 10. Pipeline processing of the FFX scheme ($1\hat{k}$ -point FFT, 8-point IFFT, $4\hat{k}$ -point FFT).

being divided into three parts: 32-point FFT, 32-point FFT, and 16-point FFT (see figure 9). The input signals are multiplied by the window function between the input buffer and FFT, so that the input buffer size is based on the 3-bit signals. FFT is realized by changing the twiddle factor according to the processing stages. This helps minimize the ROM of the twiddle factors.

5.2.4. F-Block (FFX mode)

The FFX mode is shown in figure 10. The first-stage FFT ($1\hat{k}$ -point FFT) is performed in the same manner as $32 \text{ points} \times 32 \text{ points}$ of FX mode.

The second-stage FFT ($4\hat{k}$ -point FFT) is serially processed with one butterfly computing unit. Since 2×8 -point data is obtained every single process of $1\hat{k}$ -point

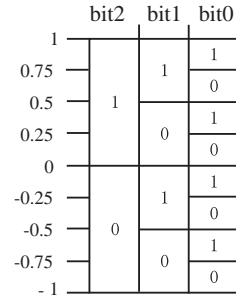


Fig. 11. Sampling bit level.

3-bit Length		2-bit		1-bit (H)		1-bit (M)	
Code	Weight	Code	Weight	Code	Weight	Code	Weight
000	-0.875	00X	-0.750	0XX	-0.500	X0X	-0.500
001	-0.625						
010	-0.375						
011	-0.125	01X	-0.250	1XX	0.500	X1X	0.500
100	0.125						
101	0.375						
110	0.625	11X	0.750				
111	0.875						

Fig. 12. Sampling bit level at 3-bit length.

first-stage FFT, 4096-point data is obtained by repeating the process of the first-stage FFT 256 times. The required time for this process is: $512 \times 256 = 128\hat{k}$ [CLK]. On the other hand, the required time for the process of 4096-point FFT using one butterfly computing unit is:

$$4096 \times \log_2(4096)/2 = 24\hat{k} \text{ [CLK]}. \quad (23)$$

Compared with these processing times, the processing time of 4096-point FFT with one butterfly computing unit is much shorter.

5.2.5. Window function processing

After re-allocated to two datasets, the signals are multiplied by window function. Any of the following window functions are selected: None (rectangular window), Hanning, Hamming, and Blackman. Window functions are generated in the CPU according to the selected command ("WINDOW") from the Monitor & Control Computer before the correlation process starts.

5.2.6. Data conversion

The input signals go through 3-bit processing. By setting a command ("SMPLBIT") from the Monitor & Control Computer, the input signals are processed as 1-bit or 2-bit data. Also, conversion to 1-bit data with (M) middle bit only is available. Assumed threshold value for each bit of sampling data is given as shown in figure 11. Based on the above threshold value, converted value of the input data is calculated as shown in figure 12. The input signals are converted into 16-bit floating point operation format before FFT.

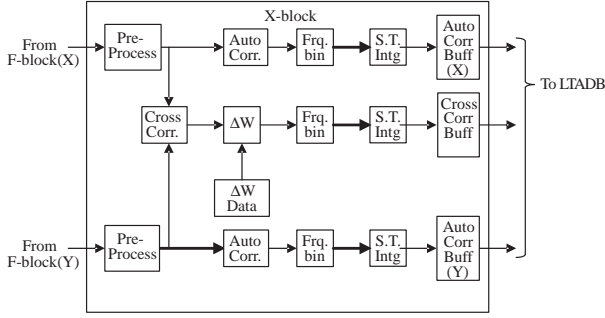


Fig. 13. Block diagram of the correlation in a FX mode.

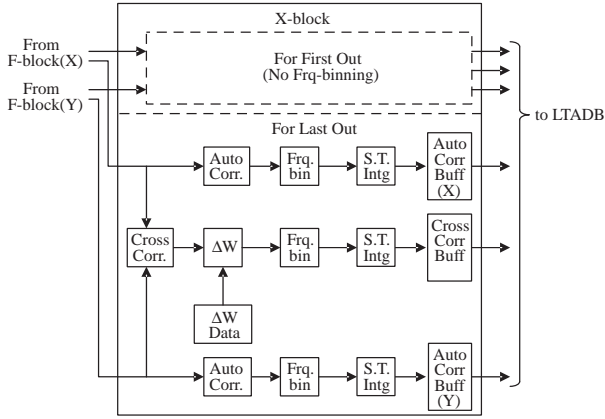


Fig. 14. Block diagram of the correlation in a FFX mode.

5.2.7. X-block (FX mode)

The composition of X-block in normal FX processing is shown in figure 13. Correlation processing is performed in $8\hat{k}$ -channel either of USB or LSB. For improving the sensitivity loss (see table 6 of Okumura et al. 2001), 2-channel frequency binning is performed to generate $4\hat{k}$ -channel data (Frq. bin). Integration of 100 milliseconds is conducted in time integration (S.T.Intg). If the integration takes longer than 100 milliseconds, it is performed in the Long-Term Accumulation and Output Board (LTAOB) at the time of 16-parallel data synthesis.

In OTF mode, the data is compressed from $8\hat{k}$ frequency channels to 32 frequency channels by frequency binning. With time component of 1 millisecond, the correlation buffer area is changed every 1 millisecond. The output to the Long-Term Accumulation and Output Board (LTAOB) is performed every 100 millisecond.

Prior to the correlation processing, the data from the F-block needs some pre-processing such as split of two datasets, USB/LSB (upper and lower sideband) selection, and 90-degree and 180-degree phase switching demodulations. In splitting process of two datasets, the input data are added and subtracted, and then the two-data components combined in the F-block are split. When LSB is selected, the sign of the split Imag component is inverted. On the other hand, when USB is selected, the split data is sent to the correlation process without any additional

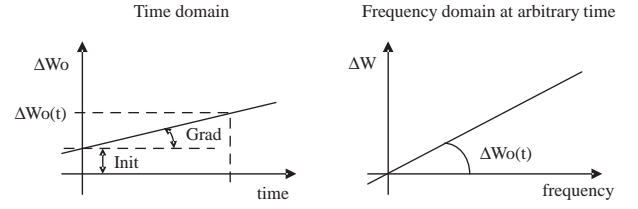


Fig. 15. ΔW correction.

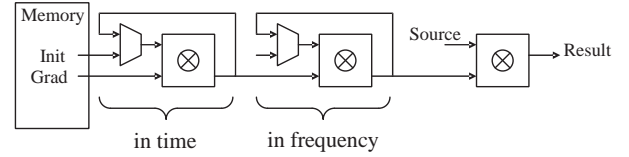


Fig. 16. ΔW correction circuit.

processing. In 90-degree and 180-degree phase-switching demodulations, switching between Real and Imag, and sign inversion are performed according to the two phase-switching signals.

5.2.8. X-block (FFX mode)

X-block in the FFX processing is shown in figure 14. In the FFX processing, X-block has a dual structure considering the processing speed of the device. The first-stage FFT is the same as that of FX mode, however frequency binning is not performed. Split of two datasets in the second-stage FFT is not performed in X-block, since the process is performed in F-block. The results of the second stage FFT are output together with USB and LSB. Two-channel frequency binning is performed for improving the sensitivity loss (see table 6 of Okumura et al. 2001).

5.2.9. ΔW correction

ΔW correction is performed based on the baseline. ΔW correction coefficient is generated within FPGA. Firstly, $\Delta W_0(t)$, the gradient of ΔW to time change, is evaluated and then the value of each frequency channel is calculated (see figure 15). Circuit diagram of the line graphs above is shown in figure 16.

For every 1 millisecond, the initial value (Init) is provided by the Monitor & Control Computer, and read as a initial gradient [$\Delta W_0(0)$]. In the border between segments, the previous value is multiplied by the gradient (Grad) data to generate a gradient of a new segment [$\Delta W_0(t)$]. In the arbitrary time (t), initial value (the value of DC) is set to 0. ΔW is set for every 128 channel in the full bandwidth of $8\hat{k}$ channel, which means the full bandwidth ($8\hat{k}$ channel) is corrected with 64 steps. The initial value of $\Delta W_0(t)$ can be set for every 1 millisecond, however, a given value is set within 128 channel. The gradient of $\Delta W_0(t)$ is the gradient variation of ΔW per one segment length for FFT. The Monitor & Control Computer specifies a set of the initial value and gradient approximately every 1 second.

Table 4. Operation mode in a FX mode.

Bandwidth	Spectral points	Spectral resolution	Velocity resolution at 1 mm	Correlation
4096 MHz	4096	1 MHz	1.0 km s ⁻¹	2AC-1CC
2048 MHz	4096	0.5 MHz	0.5 km s ⁻¹	4AC-1CC

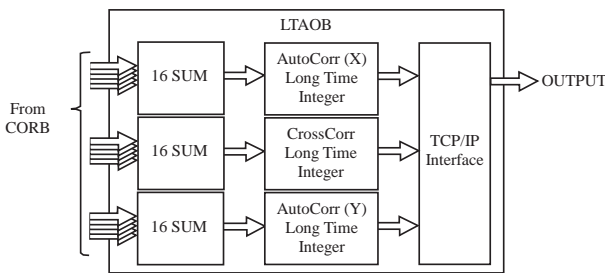
Table 5. Operation mode in a FFX mode.

Stage	Bandwidth	Spectral points	Spectral resolution	Velocity resolution at 1 mm	Correlation
1 st	4096 MHz	512	8 MHz	8.0 km s ⁻¹	2AC-1CC
2 nd	64 MHz	2048	31.25 kHz	0.031 km s ⁻¹	2AC-1CC
1 st	4096 MHz	512	8 MHz	8.0 km s ⁻¹	2AC-1CC
2 nd	128 MHz	4096	31.25 kHz	0.031 km s ⁻¹	1AC
1 st	2048 MHz	512	4 MHz	4.0 km s ⁻¹	4AC-2CC
2 nd	32 MHz	2048	15.625 kHz	0.016 km s ⁻¹	4AC-2CC
1 st	2048 MHz	512	4 MHz	4.0 km s ⁻¹	2AC-1CC
2 nd	64 MHz	4096	15.625 kHz	0.016 km s ⁻¹	2AC-1CC
1 st	2048 MHz	512	4 MHz	4.0 km s ⁻¹	2AC-1CC
2 nd	128 MHz	8192	15.625 kHz	0.016 km s ⁻¹	1AC
1 st	2048 MHz	512	4 MHz	4.0 km s ⁻¹	2AC-1CC
2 nd	96 MHz	6144	15.625 kHz	0.016 km s ⁻¹	1AC
2 nd	32 MHz	2048	15.625 kHz	0.016 km s ⁻¹	1AC

4AC: Auto-Correlation (H₁H₁ and V₁V₁, H₂H₂ and V₂V₂), 2CC: Cross-Correlation (H₁V₁, H₂V₂)

2AC: Auto-Correlation (HH and VV), 1CC: Cross-Correlation (HV)

1AC: Auto-Correlation (HH or VV).

**Fig. 17.** Long-Term Accumulation/Output Board.

5.3. Long-Term Accumulation/Output Board (LTAOB)

Final correlation value is calculated by adding the output of 16 correlators. The composition of the Long-Term Accumulation/Output Board (LTAOB) is shown in figure 17. When the correlation result is output, the data is converted into the format of IEEE single-precision floating point.

In the FX processing, the number of the output frequency channels is normally $4\hat{k}$ ($=4096$). Thus the output

data size per one correlation is

$$4\hat{k} \times 32 \times 2 \times 3 = 768\hat{k} \text{ bits}, \quad (24)$$

where 32 is the number of single-precision floating bits, 2 is the complex, and 3 is the number of correlations; auto-correlations of x and y , and a cross-correlation between them. Assuming the minimum integration time is 0.1 second, the estimated output speed is approximately 7.7 Mbps. In the FFX processing, the number of the output frequency channels is $512 + 2\hat{k}$, thus the data size per one correlation is $480\hat{k}$ bits. Consequently, the estimated output speed with 0.1-second integration time is approximately 4.8 Mbps. Correlation results are sent to the Monitor & Control Computer using TCP/IP protocol of 100 BaseT-Ether.

5.4. Operation mode

The FFX correlator are divided into four F parts in principle (not physically). Each F part in a FX mode and the first FFT stage of FFX mode are operated at 2048 MHz, and each F part at the second FFT stage of FFX mode are operated at 32 MHz. Also, the digital

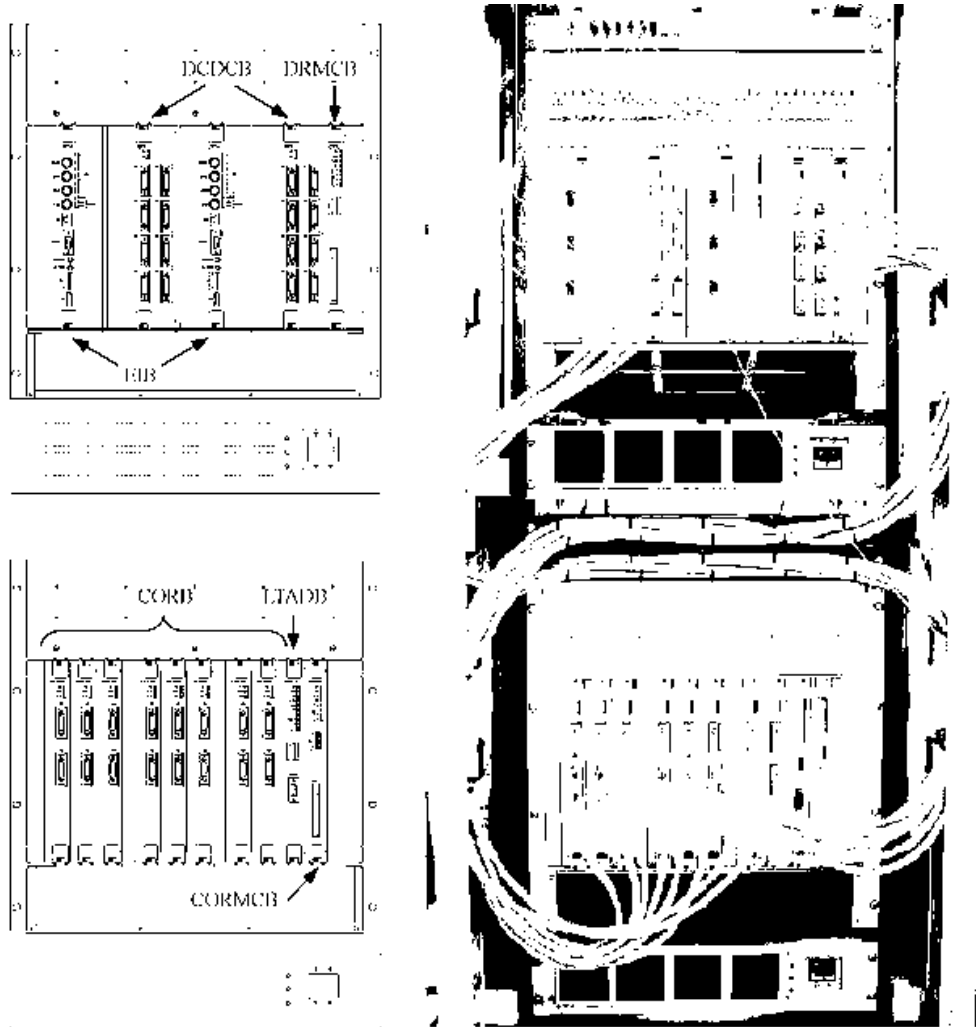


Fig. 18. FX correlator under development. There are two modules: one is the DTS-R module (top: left is a drawing of the front view, and right is a photograph), having a size of (W) 490 mm \times (H) 500mm \times (D) 500 mm; the other one is the Correlation module (bottom: left is a drawing of the front view, and right is a photograph), having a size of (W) 490 mm \times (H) 500mm \times (D) 500 mm. The total size of the GDFB is (W) 490 mm \times (H) 1100mm \times (D) 500 mm, including the two power supply modules.

signals input from EIB are distributed to arbitrary F parts by using the command (“FCHSEL”) from the Monitor & Control Computer. In FX mode and the first FFT stage of FFX mode, the digital signals of 8192 Msps are operated by combining two F parts ($= 2 \times 2048$ MHz), while the signals of 4096 Msps are operated by using one parts ($= 1 \times 2048$ MHz). At the second FFT stage of FFX mode, the digital signals of 8192 Msps are operated by combining two F parts ($= 2 \times 32$ MHz), while the signals of 4096 Msps are operated using only one parts ($= 1 \times 32$ MHz). By using the command (“FCHSEL”), the effective bandwidth after the second FFT stage can be changed.

All of the operation modes available in this FFX correlator are listed in table 4 and 5.

5.5. Hardware of the FX Correlator

The Hardware of the FX Correlator is shown in figure 18. The DTS-R module consists of two Electrical input Interface Boards (EIBs), two Delay Correction and

Data Configuration Boards (DCDCBs), and one DTS-R Monitor & Control Boards (DRMCBs). The Correlation module consists of eight Correlation Boards (CORBs), Long-Term Accumulation/Output Board (LTAOB), and one Correlation Monitor & Control Board(CORMCB). Each module is connected to the independent Power module.

The power consumption of the filter module is 400 W, while that of the output module is 600 W. The total AC power is 750 W at 1-phase 100-220 VAC 50/60 Hz (100 V $\pm 10\%$ or 220 V $\pm 10\%$). The total weight is 71.3 kg.

5.6. Evaluation and Discussion

Figure 19 shows a block diagram of the measurement setup of the frequency response of the FFX Correlator. To investigate the frequency response, it is useful to use the CW signal, which can measure the folding effects by sweeping the frequency range of 0 to 4096 MHz. The white noise is important to measure the frequency response, be-

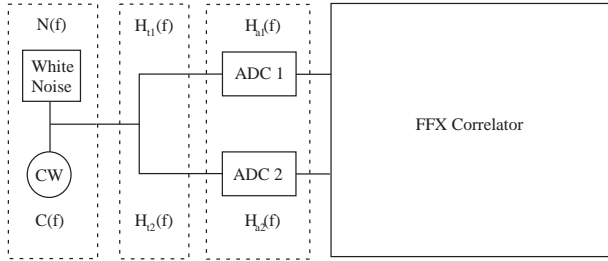


Fig. 19. Block diagram of the measurement setup. A detailed block diagram of the FFX correlator is shown in figure 3. The white noise is generated by the ASTE analog backend subsystem, while the CW signal is produced by the Agilent E4440B, which is locked in phase to a standard signal of 10 MHz generated by the reference clock generator. The ADC 1 and ADC 2 with 8192 Msps are also locked in phase to a signal of 8192 MHz generated by the reference clock generator. Note that the ADCs were developed specifically for ASTE (Okuda et al. 2008), and all output signals from the reference clock generator are generated by the built-in 5MHz crystal oscillator (OCXO).

cause the astronomical signals obey the Gaussian random variable. To obtain the input signals that are approximated to the zero-mean Gaussian probability, mixing of the CW signal with the white noise is necessary.

The frequency response of the FFX correlator when CW is included is written as

$$P_{\text{on}}(f) = a_{\text{on}} \cdot [|C(f)|^2 + |N(f)|^2] \cdot |H_1(f)H_2^*(f) \cdot |H_D(f)|^2, \quad (25)$$

where $C(f)$ is the frequency response of the CW signal, $N(f)$ is the frequency response of the white noise from the ASTE analog backend subsystem, H_1 and H_2 are the frequency response by different transmission paths, in which $H_1 = H_{t1}H_{a1}$ and $H_2 = H_{t2}H_{a2}$ (see figure 19), and H_D is the frequency response of the FFX correlator, including the effects of requantization and the folding noise after downsampling. The bandpass calibration is essential for estimating the CW power accurately, because the bandpass response becomes a time-variable due to outdoor air temperature. The frequency response without the CW signal is written as

$$P_{\text{off}}(f) = a_{\text{off}} \cdot |N(f)|^2 \cdot |H_1(f)H_2^*(f) \cdot |H_D(f)|^2. \quad (26)$$

The ADCs work as 1-bit performance (Okuda et al. 2008). In that case, it is important to adjust the power as precisely as possible so as to avoid the high-order spurious effects. The frequency responses of $P_{\text{on}}(f)$ and $P_{\text{off}}(f)$ depend on the relative power of the CW signal to the white noise, and also the threshold levels in quantization. To correct these effects, we need to calibrate the bandpass by sensitively adjusting the continuum floor level of P_{off} to that of P_{on} in the data analysis. These values are a_{on} and a_{off} .

From equations (25) and (26), the frequency response in a FFX mode is written as

$$P_{\text{on}}^F(f) = a_{\text{on}} \cdot [|C(f)|^2 + |N(f)|^2] \cdot |H_1(f)H_2^*(f) \cdot |H_D^F(f)|^2 \quad (27)$$

while the frequency response without the CW signal can be written as

$$P_{\text{off}}^F(f) = a_{\text{off}} \cdot |N(f)|^2 \cdot |H_1(f)H_2^*(f) \cdot |H_D^F(f)|^2, \quad (28)$$

and then the CW frequency response including the response of the measurement system is derived as

$$P^F(f) = P_{\text{on}}^F - P_{\text{off}}^F \cdot \frac{a_{\text{on}}}{a_{\text{off}}} = a_{\text{on}} \cdot |C(f)|^2 \cdot |H_1(f)H_2^*(f) \cdot |H_D^F(f)|^2. \quad (29)$$

Similarly, the frequency response in a FX mode is written as

$$P_{\text{on}}^N(f) = a_{\text{on}} \cdot [|C(f)|^2 + |N(f)|^2] \cdot |H_1(f)H_2^*(f) \cdot |H_D^N(f)|^2 \quad (30)$$

while the frequency response without the CW signal can be written as

$$P_{\text{off}}^N(f) = a_{\text{off}} \cdot |N(f)|^2 \cdot |H_1(f)H_2^*(f) \cdot |H_D^N(f)|^2, \quad (31)$$

and then the CW frequency response including the response of the measurement system is derived as

$$P^N(f) = P_{\text{on}}^N - P_{\text{off}}^N \cdot \frac{a_{\text{on}}}{a_{\text{off}}} = a_{\text{on}} \cdot |C(f)|^2 \cdot |H_1(f)H_2^*(f) \cdot |H_D^N(f)|^2. \quad (32)$$

From equations (29) and (32), we can derive the frequency response in a FFX mode from the correlated spectra obtained in FFX and FX modes as

$$|H_D^F(f)|^2 = \frac{P^F(f)}{P^N(f)} \cdot |H_D^N(f)|^2. \quad (33)$$

Since the frequency response of $H_D^N(f)$ in the FX mode is well known (Thompson et al. 2001), the frequency response in a FFX mode can be derived finally.

Figure 20 shows the frequency response of the FFX correlator at a bandwidth of 64 MHz in the range of 2048 to 2112 MHz, and that the lower limits of about -33 dB to -40 dB are successfully measured with this method. The measurement frequency resolution was 31.25 kHz. The measurement results show that the effective bandwidth is about 59.28 MHz, which was obtained by the passband responses of about -1 dB at 2046.40625 and 2106.28125 MHz, -3 dB at 2045.3125 and 2107.28125 MHz, and by a stopband response with the first sidelobe of about -20 dB. The measurement results are well consistent with the theoretical curve in the passband, both bandedges (sharpness), and first sidelobe levels. In the stopband response except these responses, however, it is shown that there are differences between theoretical curve and measured results. This problem is probably due to the non-linear response of 1-bit ADC and the precision of the data reduction process in this measurement method. The cross-modulation distortion is strongly generated in digitizing the CW signals at 1 bit. This character complicates the data reduction method, and will reduce the measurement precision. If the ADCs with 3 bits or more are feasible, this problem will be relaxed.

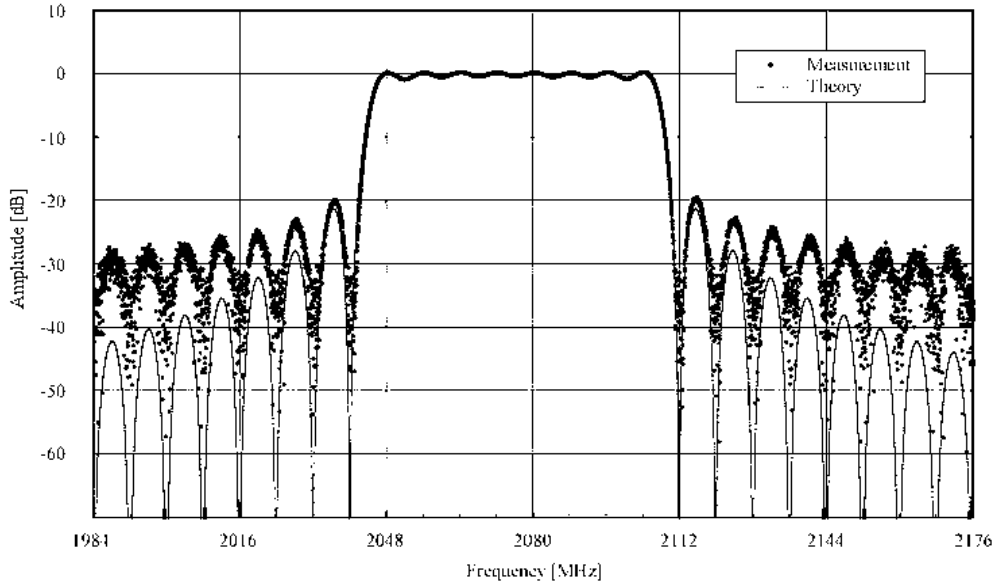


Fig. 20. The measured frequency response of the FFX correlator at a bandwidth of 64 MHz in a frequency range of 2048 to 2112 MHz. First sidelobe of about -20 dB and other stopband response of better than -23 dB were successfully achieved. A comparison between the measured frequency response of the FFX correlator (points) and the ideal frequency response of the FFX scheme (full line) in a rectangular window function without zeroing [see equations (14) and (11)] are shown.

Finally, the measurement results show that the theory of the FFX scheme can be confirmed, and the development of the FFX Correlator was successfully realized.

6. Summary

There are two basic designs of a digital correlator: the XF-type in which the cross-correlation is calculated before Fourier transformation, and the FX-type in which Fourier transformation is performed before cross multiplication. To improve the FX-type correlator, we established a new algorithm for correlation process, that is called the FFX scheme. The FFX scheme demonstrates that the realization of a stopband response with first and second sidelobes of -34 dB and higher-order sidelobes of -60 dB is technically feasible. The FFX scheme consists of 2-stage Fourier Transform blocks, which perform the 1st-stage Fourier Transform as a digital filter, and the 2nd-stage Fourier Transform to achieve higher dispersion. The FFX scheme provides flexibility in the setting of bandwidth within the sampling frequency.

The input data rate of the developed FFX correlator is about 48 Giga bit per second (Gbps) with 3-bit quantization at the sampling frequency of 8192 or 4096 Msps, which is 8192 Msps \times 3 bits \times 2 IF or 4096 Msps \times 3 bits \times 4 IFs. We have successfully evaluated the feasibilities of the FFX correlator hardware. Also, this hardware will be

installed and operated as a new spectrometer for ASTE.

We successfully developed the FFX correlator, measured its performances, and demonstrated the capability of a wide-frequency coverage and high-frequency resolution of the correlation systems. Our development and measurement results will also be useful and helpful in designing and developing the next generation correlator.

Acknowledgments

The authors would like to acknowledge Yoshihiro Chikada for his helpful technical discussions. The author would like to express gratitude to Brent Carlson who provided constructive comments and suggestions on this paper. This research was partially supported by the Ministry of Education, Culture, Sports, Science and Technology, Grant-in-Aid for Young Scientists (B), 17740114, 2005.

References

- Bunton, J, 2000, ALMA Memo 342, (Charlottesville: NRAO)
- Bunton, J, 2003, ALMA Memo 447, (Charlottesville: NRAO)
- Carlson, B. 2001, NRC-EVLA Memo 014
- Chikada, Y., Ishiguro, M., Hirabayashi, H., Morimoto, M., Morita, K., Kanzawa, T., Iwashita, H., Nakazima, K., et al. 1987, Proc. IEEE, 75, 1203
- Escoffier, R. P., Comoretto, G. Webber, J. C., Baudry, A., Broadwell, C. M., Greenberg, J. H., R. R. Treacy, R. R.,

- Cais, P., et al. 2007, *A&A* 462, 801
- Ezawa, H., Kawabe, R., Kohno, K., Yamamoto, S. 2004, *SPIE* 5489, 763
- Iguchi, S., Okuramu, S. K., Okiura, M., Momose, M., Chikada, Y. *URSI General Assembly (J6:RECENT SCIENTIFIC DEVELOPMENTS)*, Maastricht, 2002.
- Iguchi, S., Kurayama, T., Kawaguchi, N., & Kawakami, K. 2005, *PASJ* 57, 259
- Narayanan, D., Groppi, C. E., Kulesa, C. A., & Walker, C. K. 2005, *ApJ*, 630, 269
- Okuda, T., Iguchi, S. 2008, *PASJ* 60, 315
- Okumura, S. K., Chikada, Y., Momose, M., Iguchi, S. 2001, *ALMA Memo No.350* (Charlottesville: NRAO)
- Rabiner, L. R., Schafer, R. W. 1971, *IEEE Trans. Audio Electroacoust.*, AU-19, 200
- Thompson, A. R., Moran, J. M., & Swenson, G. W.Jr. 2001, *Interferometry and Synthesis in Radio Astronomy*, 2nd Ed., (New York:John Wiley & Sons), 289
- Weinreb, S. 1963, *Digital Spectral Analysis Technique and Its Application to Radio Astronomy*, (R. L. E., MIT, Cambridge, Mass.), Tech. Rep. No. 412